Astronomy & Astrophysics manuscript no.
(DOI: will be inserted by hand later)

September 7, 2004

Relative abundance pattern along the profile of high redshift Damped Lyman-α systems*

E. Rodríguez[1], P. Petitjean[1,2], B. Aracil[1], C. Ledoux[4], and R. Srianand[5]

[1] Institut d'Astrophysique de Paris, UMR 7095, 98 bis Boulevard Arago, 75014 Paris, France
[2] Observatoire de Paris, LERMA, UMR 8112, 61 Avenue de l'Observatoire, 75014 Paris, France
[3] European Southern Observatory, Alonso de Cordova 3107, Casilla 19001, Vitacura, Santiago, Chile
[4] IUCAA, Post Bag 4, Ganesh Khind, Pune 411 007, India

Abstract. We investigate abundance ratios along the profiles of six high-redshift Damped Lyman-α systems, three of them beeing associated with H_2 absorption. We use a new method to derive optical depths in each velocity pixel. The variations of the pixel abundance ratios are found to be remarquably small and usually smaller than a factor of two within a profile. This results holds when considering independent sub-clumps in the same system. Only in the components where H_2 is detected is the depletion factor significantly enhanced. There is a strong correlation between [Fe/S] and [Si/S] ratios showing that the abundance ratio patterns are definitely related to the presence of dust. The depletion pattern is usually close to that seen in warm halo gas of our Galaxy.

Key words. Cosmology: observations- Quasars: absorption lines - Quasars: individual: Q 0528−250, Q 0013+004, Q 1037−270, Q 1157+014, Q 0405−443

1. Introduction

Damped Lyman-α systems (hereafter DLAs) observed in QSO spectra are characterized by strong H Iλ1215 absorption lines with broad damping wings. Although the definition has been restricted for historical reasons to absorptions with log N(H I) > 20.3 (Wolfe et al. 1986), damping wings are easily detected in present day high quality data for much lower column densities (down to log N(H I) $\sim$ 18.5). A more appropriate definition should be related to the physical state of the gas. If we impose the condition that the gas be neutral, then the definition should be limited to systems with log N(H I) > 19.5 (e.g. Viegas 1995).

Since their discovery twenty years ago (Wolfe et al., 1986), it is clear that DLAs have something to do with galaxy formation. It is a matter of debate however to what kind of galaxy DLAs are associated. Some authors identify these systems with large rotating disks (Prochaska & Wolfe, 1997; Hou, Boissier, & Prantzos, 2001), while others think that DLAs arise mostly in dwarf galaxies (Centurion et al., 2000), or galactic building blobs (Haehnelt, Steinmetz, & Rauch, 1998; Ledoux et al., 1998). The answer is probably not unique. DLAs represent however the major reservoir of neutral hydrogen at any redshift, (Storrie-Lombardi & Wolfe, 2000) and probe the chemical enrichment and evolution of the neutral Universe (see Pettini et al. 1994; Lu et al. 1996; Prochaska et al. 1999; Ledoux et al. 2002a and references therein). It is well known that abundances can be measured very accurately in DLAs. It is therefore possible to discuss the connection between observed abundance ratios and dust content and to trace the nucleosynthesis history of the dense gas in the universe.

In this context, it is helpful to compare the results with measurements in the ISM of our Galaxy. Refractory elements that condense easily into dust grains - namely, Cr, Fe, Ni- are strongly depleted (up to a factor hundred) in the ISM, while non-refractory elements remain in its gaseous phase - S, Zn, and partially Si-. The amount of depletion depends on the physical condition of the gas. Thus, different depletion patterns are observed depending whether the gas is cold or warm and/or whether the gas is located in the disk or the halo of the Galaxy (Savage & Sembach, 1996). The LMC and SMC also exhibit different gas-phase abundance ratios (Welty et al., 1999). However, a particular nucleosynthesis history can give rise to peculiar metallicity patterns and mimic the presence of dust. Tinsley (1979) suggested that type Ia supernovae are the major producers of Fe and an enhancement in [α/Fe] ra-

---

Send offprint requests to: E. Rodriguez, rodrig@iap.fr

* Based on observations carried out at the European Southern Observatory (ESO), under progs. ID 65.O-0063, 66.A-0624, 67.A-0078, 68.A-0106 and 68.A-0600, with the UVES echelle spectrograph installed at the Very Large Telescope (VLT) unit KUEYEN on Mount Paranal, Chile.

tios, -α-elements being mostly O, S, Si- could reflect an IMF skewed to high masses and therefore the predominant role of type II supernovae. For very low metallicity stars ([Fe/H] < -3) in the Galaxy, large variations in several abundance ratios have been reported (McWilliam, 1997), suggesting that peculiar nucleosynthesis processes and inhomogeneous chemical enrichment probably take place.

As mentioned above, DLAs trace the chemical evolution of galaxies at early epochs in the Universe. Many detailed studies have been performed so far, revealing that their metallicities range between 1/10 and 1/300 $Z_\odot$, and they show quite "uniform" abundance patterns that are compatible with low dust content (see Pettini et al. 1994, Lu et al. 1996, Prochaska et al. 1999, Ledoux et al. 2002a). This uniformity in the relative abundance patterns observed from one DLA to the other has been emphasized by Prochaska & Wolfe (2002) and suggests protogalaxies have common enrichment histories.

Few studies have adressed the question of the homogeneity inside each particular system. Prochaska & Wolfe (1996) first studied chemical abundances variations in a single DLA. They showed that the chemical abundances were uniform to within statistical uncertainties. Lopez et al. (2002) confirmed this findings from the analysis of another DLA using Voigt profile decomposition. Petitjean et al. (2002) and Ledoux et al. (2002b) showed that the depletion patterns in subcomponents were very similar along DLA profiles except in the components where molecular hydrogen is detected and where depletion is larger. More recently, Prochaska (2003), have performed a study over 13 systems concluding the majority of DLAs have very uniform relative abundances. This is in contrast in particular with the dispersion in nucleosynthetic enrichment of the Milky Way as traced by stellar abundances.

Here, we use the best data from our survey of DLAs (Ledoux et al. 2003) to investigate further this issue using an inversion method to derive the velocity profiles in different abundance ratios. In particular we investigate the consequence of the presence of molecular hydrogen in some of the DLAs. The paper is structured as follows : we describe the data in Section 2; in Section 3 we briefly introduce the method used for the analysis; results are presented and discussed in Sections 4 and 5. ??.

2. Observations and Sample

As emphasized by Prochaska (2003), high S/N ratio is needed to investigate pixel by pixel variations. In addition, we want to investigate the difference between systems where molecular hydrogen is detected and where it is not detected because it has been shown (e.g. Petitjean et al. 2002) that depletion is larger in components where H_2 is detected. We therefore restrict the sample to the six highest S/N ratio spectra from the list of 34 quasars observed during the VLT survey for molecular hydrogen in DLAs (Ledoux et al. 2003). The QSO have been observed with the Ultraviolet and Visible Echelle Spetctrograph (D'Odorico et al., 2000), mounted on the 8.2 m KUEYEN telescope operated at Cerro Paranal, Chile, during the observation periods P65 to P68. The resulting resolution is $\sim$ 42000 for all the spectra and S/N ratio is larger than 50 per pixel (see Ledoux et al. 2003 for details). For Q 0528−250, we have also retrieved data from the public UVES ARCHIVE of ESO, obtaining a very high quality spectra with SNR $\sim$ 100.

Molecular hydrogen has been detected in three of these systems. This is the case for Q 0013−004 (Petitjean et al., 2002), Q 0528−250 (Srianand & Petitjean, 1998) and Q 0405−443 -system at $z_{abs} = 2.595$- (Ledoux et al. 2003). The six systems span a wide range of H I column densities from log N(H I) = 19.7 up to 21.80. In all systems we chose to analyse absorption features that are well defined and do not suffer from major blending.

The main characteristics of these systems are decribed below and summarized in Table 1. We use the standard definition [X/H] = (log N(X) − log N(H I)) − log $Z_\odot$(X) with log $Z_\odot$(X) beeing the solar metallicity of species X taken from Savage & Sembach (1996).

2.1. Q 0013−004

The presence of H_2 at $z_{\rm abs} = 1.973$ was first reported by Ge & Bechtold (1997). Spread over more than 1000 km s^{-1} (see Figure 7), this system is the DLA absorber with the highest molecular fraction known so far ($-2.7 < f(H_2) < -0.64$, Petitjean et al. 2002) for log N(H I) = 20.83.

Molecular hydrogen is detected in four different components spread all over the system, at relative velocities, ~ -572, ~ -480, ~ 0 and $\sim +80$ km s^{-1}. Petitjean et al. (2002) report also four additionnal strong metal components which have probably a non negligible contribution to the total H I column density.

The same authors show that the presence of H_2 is closely related to the physical conditions of the gas. They analyse the C I and C I* transitions seen in the four molecular components. From the C I*/C I ratio and the excitation temperature deduced from the different rotational H_2 J levels column densities, they conclude that the density of the gas is high ($n_{\rm H} > 30$ cm^{-3}) and the temperature is low (70 K). They suggest that the large variations from one component to the other seen in the excitation of the different J levels are due to an inhomogeneous UV radiation field.

Finally, they perform a component by component analysis of the different species, concluding that all components have similar abundance ratios and depletion factors independently of the presence or absence of H_2. Only for the special molecular component at $z_{\rm abs} = 1.97296$ the dust depletion turns to be important. The depletion of Fe is comparable to that observed in the cold interstellar medium of the Galactic disk. We summarize in Table 3 the overall abundances of the principal elements present in the system. We also confirm the strong depletion of the ~ 480 km s^{-1} component.

Quasar	$z_{\rm em}$	$z_{\rm abs}$	log$N$(H I)$^{\rm a}$	log$N$(H$_2$)	[Fe/H]	Metallicity
0013 − 004	2.09	1.973	20.83	17.72	-1.46 ± 0.01	-0.68 ± 0.03
0405 − 443	3.00	2.595	20.90	18.16	-1.30 ± 0.10	-0.93 ± 0.02
0405 − 443	3.00	2.549	21.00	< 13.9	-1.49 ± 0.01	-0.96 ± 0.04
0528 − 250	2.80	2.811	21.35	18.22	-1.44 ± 0.01	-1.07 ± 0.01
1037 − 270	2.31	2.139	19.70	< 13.7	-0.51 ± 0.03	-0.19 ± 0.02
1157 + 014	1.99	1.944	21.80	< 14.5	-1.84 ± 0.03	-1.41 ± 0.02

Table 1. Description of the sample. The neutral and molecular hydrogen column densities are taken from Ledoux et al. (2003). Both [Fe/H] and Metallicity values are from this work and correspond to the values integrated over the systems. Metallicity is derived in all cases from [S/H] except for Q 1157 + 014 for which we have used [Zn/H] instead.

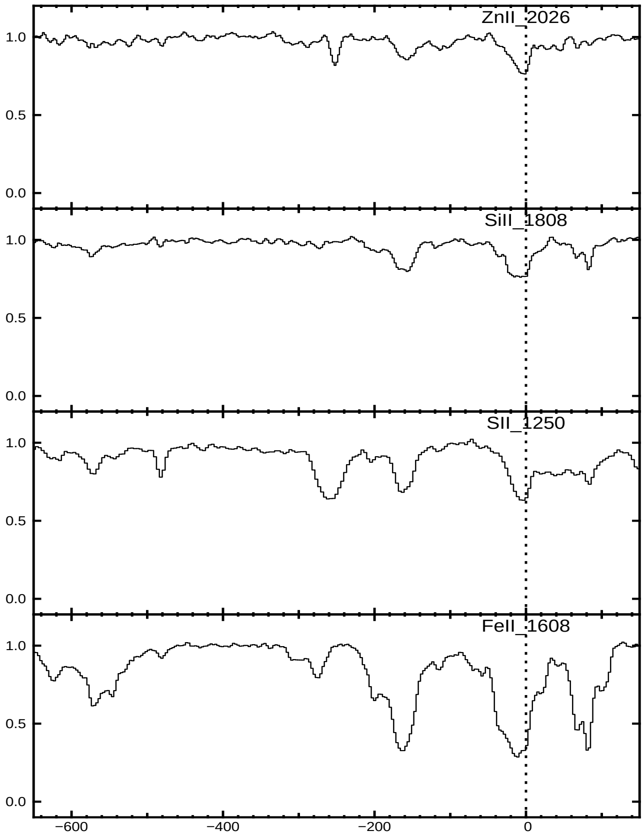

Fig. 1. Absorption spectra plotted on a velocity scale for a few transitions observed in the $z_{\rm abs}$ = 1.973 DLA system toward Q 0013−004. Molecular transitions have been detected in four components located at $v \sim -615$ km s^{-1}, $v \sim -480$ km s^{-1}, $v \sim 0$ km s^{-1} and ~ 85 km s^{-1}. (Petitjean et al., 2002)

2.2. Q 0405−443

Lopez et al. (2001) first discovered three damped systems along the line of sight to this quasar at redshifts $z_{\rm abs}$ = 2.550, 2.595 and 2.621. Later, Ledoux et al. (2003) confirmed the damped nature of these three absorptions. We adopt here their H I column density values. From the three systems observed in this line of sight we have included in our sample the systems at $z_{\rm abs}$ = 2.549, log N(H I) = 21.0, and $z_{\rm abs}$ = 2.595, log N(H I) = 20.9. Our data on the third system is not good enough to perform a reliable analysis.

Ledoux et al. (2003) detect the presence of H$_2$ at $z_{\rm abs}$ = 2.595 from J = 0, 1, 2, 3 rotational transitions. They measure log N(H$_2$) = 18.16, one of the largest H$_2$ column densities ever seen in a DLAs, although the molecular fraction in the corresponding cloud is not so large (log f(H$_2$) = −2.44) due to the high column density of neutral hydrogen. Note that C I is not detected.

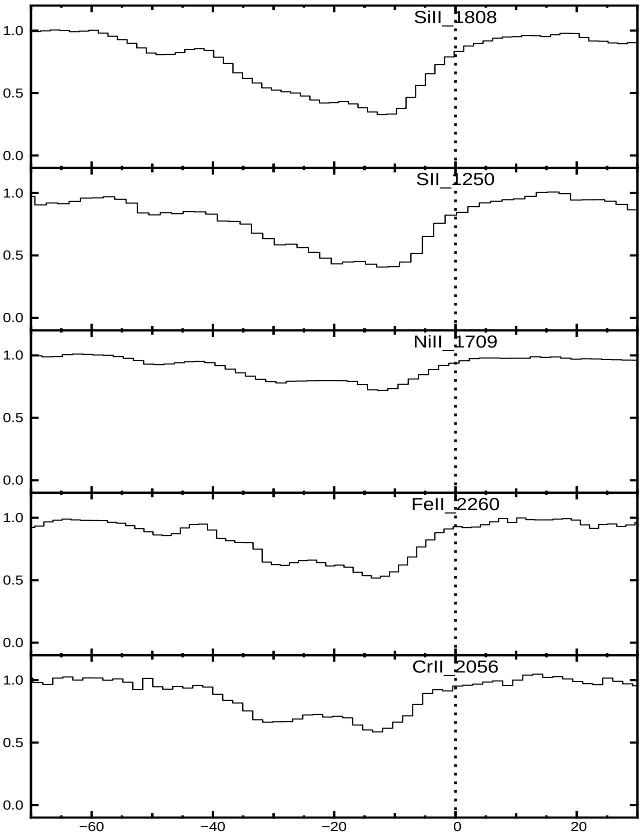

Fig. 2. Absorption spectra plotted on a velocity scale for a few transitions observed in the $z_{\rm abs}$ = 2.595 DLA system toward Q 0405−443. Numerous molecular transitions have been detected in two components located at $v \sim -24$ km s^{-1} and ~ -11 km s^{-1}. (Ledoux et al., 2003)

2.3. PKS 0528−250

We have collected all the data from the ESO ARCHIVE available on this QSO and added them together with our

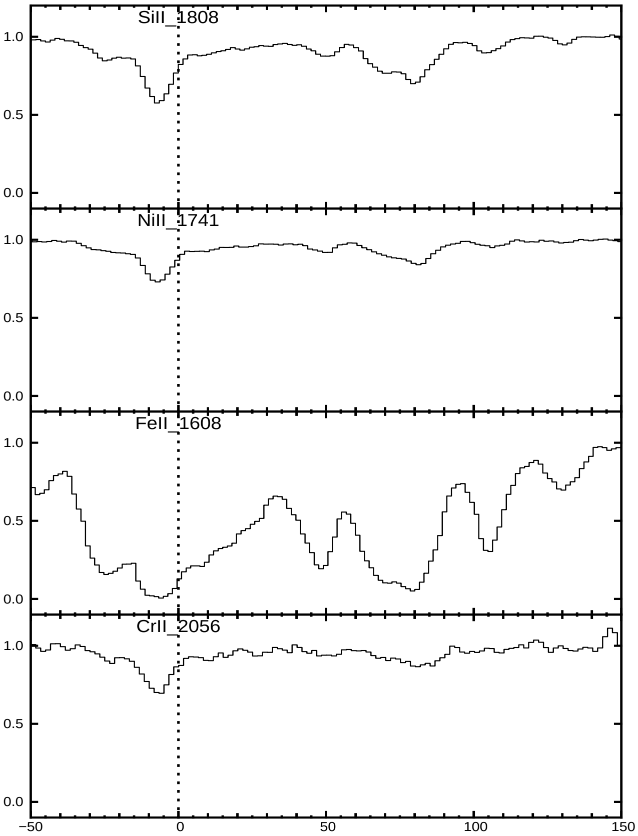

Fig. 3. Absorption spectra plotted on a velocity scale for a few transitions observed in the $z_{\rm abs}$ = 2.55 DLA system toward Q 0405−443. (Ledoux et al., 2003)

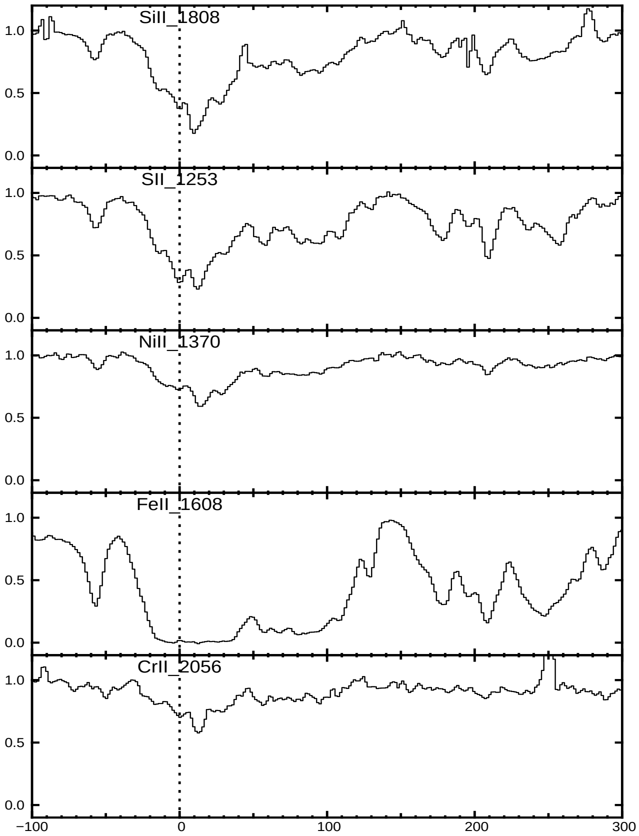

Fig. 4. Absorption spectra plotted on a velocity scale for a few low ionization species observed at $z_{\rm abs}$ = 2.811 along the line of sight to PKS 0528−250. The system extends over more than 400 km s^{-1}.

own data. The result is an very high SNR spectrum extended over the wavelength range 3000−10000 Å apart from a few gaps. The absorption redshift is slightly higher than that of the emitting source, suggesting that the absorbing system could be associated with the quasar. A useful consequence of this situation is a larger number of metallic transitions are redshifted outside the Lyman-α forest and therefore can be used for our analysis.

This system has been known for many years to be the only system at high redshift where molecules were detected, (Levshakov & Varshalovich, 1985; Songaila & Cowie, 1996; Srianand & Petitjean, 1998). New data have been obtained with VLT by Ledoux et al. (2003). The latter authors derive log N(H$_2$) = 17.93 and 18.0 in two components at $z_{\rm abs}$ = 2.81100 and 2.81112 respectively. Given the large hydrogen column density (log N(H I) = 21.35), the molecular fraction is only f(H$_2$) = 9×10^{-4}. The excitation temperature for the J = 1 rotational level is between 150 and 200 K and the density is probably quite large (Srianand & Petitjean 1998).

As mentioned by Lu et al. (1996) the metal absorption lines are unusually wide and complex, spreading over about 400 km s^{-1}. They appear to be structured in two main sub-clumps above and below +140 km s^{-1} (see Figure 4) suggesting the idea of two interacting galaxies.

2.4. Q 1037−270

The continuum of the QSO is difficult to constrain due to the presence of a complex system of BAL troughs (see Srianand & Petitjean 2001). A first limit on the neutral hydrogen column density was derived by Lespine & Petitjean (1997) from the absence of damped wings in a low resolution spectrum. We adopt log N(H I) = 19.7 from Srianand & Petitjean (2001). This is the lowest column density in our sample. However, this system has the highest metallicity known for DLAs at such redshift ($z_{\rm abs}$ = 2.139), [Zn/H] = −0.26. As a consequence of this high metallicity, many low-ionisation lines are detected, including C I, though no molecules are detected. Some of the corresponding species are shown in Figure 5.

The depletion pattern derived by Srianand & Petitjean (2001) is compatible with low dust content if any. The gas seems to be warm and halo like as we infer from the overall metallicities summarized in Table 3.

2.5. Q 1157+014

The system has the highest H I column density in our sample (log N(H I) = 10$^{21.8}$ cm^{-2} and is close to the emission redshift of the quasar. Absorption in 21 cm has been detected by Briggs et al. (1984) and the spin tem-

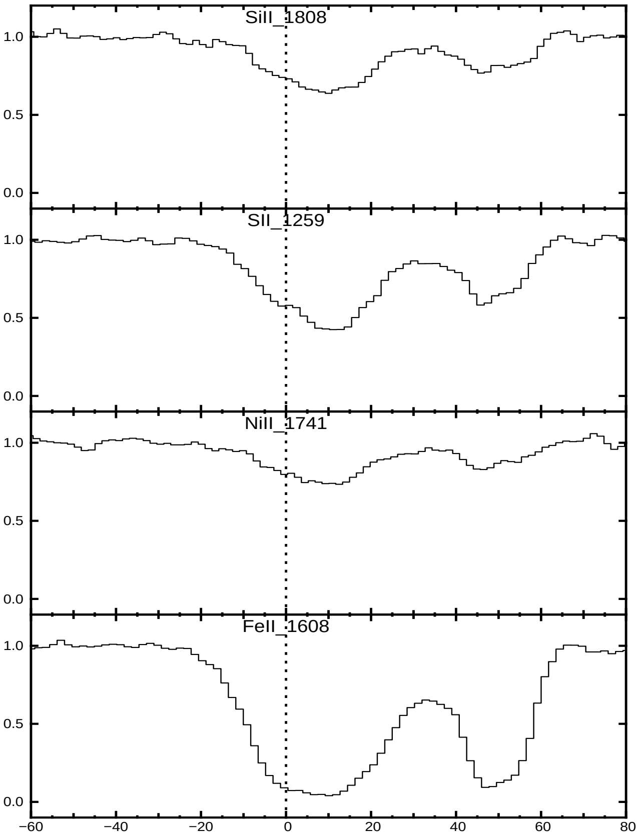

Fig. 5. Absorption spectra plotted on a velocity scale for a few transitions in the DLA system at $z_{\rm abs} = 2.139$ towards Q 1037−270. The system shows a "smooth" profile for all the elements spread over nearly 100 km s^{-1}

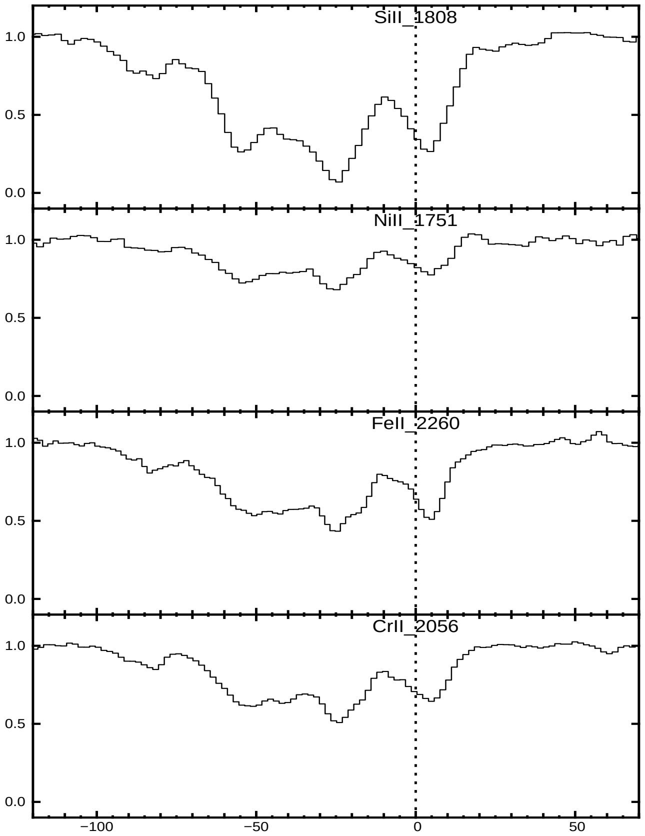

Fig. 6. Absorption spectra plotted on a velocity scale for a few transitions observed in the DLA system at $z_{\rm abs} = 1.944$ towards Q 1157+014.

perature constrained by Kanekar & Chengalur (2003) to be 865±190 K. Neither H$_2$ nor C I are detected and the metallicity is the smallest in the sample ([S/H] = −1.46, see Tables 1 and 2).

3. Analysis Method

We want to estimate the column density per unit velocity along the absorption profile of species X using several transitions. Following Savage & Sembach (1991), we can write that the apparent optical depth per unit velocity of species X in the QSO spectrum at wavelength λ for any transition of oscillator strength f and rest wavelength λ_0 is $\tau_{\rm a}(\lambda) = {\rm Ln}(1/F(\lambda))$ and the column density per unit velocity is $\log N_{\rm a}(\lambda) = \log \tau_{\rm a}(\lambda) - \log f\lambda_0 - 14.976$.

Given a set of m transitions of the same species X, we can use the duplication of the information over the different transitions to derive the optical depth profile of the species taking care, in addition, of possible blending. Let $\lambda_0^{\rm k}$ and $f^{\rm k}$ be, respectively, the laboratory wavelength and the oscillator strengh of the transition k. First, the regions corresponding to these transitions are rebinned to the smallest pixel size so that they span the same redshift range over an identical number n of pixels. Let $\lambda_{\rm i}^{\rm k}$, $F_{\rm i}^{\rm k}$ be the wavelength and the normalized flux at pixel i of the region corresponding to transition k. The value $\lambda_{\rm i}^{\rm k}/\lambda_0^{\rm k} - 1$ is independant of k, thanks to the rebin, and is the redshift at pixel i. The observed optical depth, $-\ln F_{\rm i}^{\rm k}$, is considered as the sum of the optical depth, $\tau_{\rm i}^{\rm Xk}$, of transition k and the optical depth, $\tau_{\rm i}^{\rm Bk}$, of a possible intervening absorption blended with the absorption of interest (of course in practice we will choose profiles that are apparently not blended with interlopers). As the different transitions are from the same species, the quantity $\log N_{\rm a}^{\rm k}$ (or simply $\tau_{\rm i}^{\rm Xk}/f^{\rm k}\lambda_0^{\rm k}$) is the same for all transitions k. The fitted optical depth before any instrumental convolution and without taking care of any overlaping between regions, is then:

$$\tau_{\rm i}^{\rm k} = \tau_{\rm i}^{\rm Xk} + \tau_{\rm i}^{\rm Bk} \quad \forall i \in \{1,\ldots,n\}\ ,\ \forall k \in \{1,\ldots,m\} \quad (1)$$

To simplify the notation, we use the data vector $\mathbf{O}$, of $m*n$ elements, obtained by stacking the observed flux of each regions (i.e. $F_{\rm i}^{\rm k} = \mathbf{O}_{\rm i+kn-n}$), the parameter vector $\mathbf{P}$, of $n+m*n$ elements, obtained by stacking $\tau_{\rm i}^{\rm Xk}/f^k\lambda_0^{\rm k}$ and $\tau_{\rm i}^{\rm Bk}$ (i.e. $\tau_{\rm i}^{\rm Xk}/f^k\lambda_0^{\rm k} = \mathbf{P}_i$ and $\tau_{\rm i}^{\rm Bk} = \mathbf{P}_{kn+i}$), and the fitted vector $\mathbf{F}$ corresponding to the fitted flux. The χ^2 of the fit is then:

$$\chi^2 = {\rm tr}\left([\mathbf{W}\cdot(\mathbf{O}-\mathbf{F})]^{\rm T}\cdot[\mathbf{W}\cdot(\mathbf{O}-\mathbf{F})]\right) \quad (2)$$

$$with\ \ \mathbf{F} = \mathbf{C}\cdot\exp^*(-\mathbf{M}\cdot\mathbf{P}) \quad (3)$$

The matrix $\mathbf{M}$ applies the linear relation (1) to the parameters and takes care of possible overlap between different

Table 2. Atomic data

Transition	$\lambda_{\rm vac}$ (Å)	f	Ref.
Si II λ1020	1020.6989	0.01680	a
Si II λ1190	1190.4158	0.25000	a
Si II λ1304	1304.3702	0.08630	a
Si II λ1526	1526.7070	0.12700	a
Si II λ1808	1808.0129	0.00208	a
S II λ1250	1250.5840	0.00545	a
S II λ1253	1253.8110	0.01090	a
S II λ1259	1259.5190	0.01620	a
Cr II λ2056	2056.2690	0.1050	a
Cr II λ2062	2062.2361	0.0780	a
Cr II λ2066	2066.1640	0.0515	a
Fe II λ1143	1143.2260	0.01770	a
Fe II λ1144	1144.9379	0.10600	a
Fe II λ1608	1608.4508	0.05800	a
Fe II λ1611	1611.2003	0.00136	a
Fe II λ2249	2249.8768	0.00182	a
Fe II λ2260	2260.7805	0.00244	a
Fe II λ2344	2344.2130	0.11400	a
Fe II λ2374	2374.4603	0.0313	a
Ni II λ1370	1370.1320	0.0765	b
Ni II λ1454	1454.8420	0.0300	b
Ni II λ1709	1709.6042	0.0324	b
Ni II λ1741	1741.5531	0.0427	b
Ni II λ1751	1751.9157	0.0277	b
Zn II λ2026	2026.1371	0.489	a
Zn II λ2062	2062.6604	0.256	a

References: Vacuum wavelengths from Morton (2003). Oscillator strengths: (a) Morton (2003); (b) Fedchak et al. (2000).

regions. The function exp* replaces each element of a matrix by its exponential value (i.e. $\exp^*(X)_{ij} = e^{X_{ij}}$). The matrix $\mathbf{C}$ is used to convolve the calculated flux with the instrumental profile and, finally, $\mathbf{W}$ is the inverse of the variance-covariance matrix of the data.

A regularisation constraint is added to select the solutions $\mathbf{P}$ that are correlated over a specific length l_0. The selection is done by a minimisation of the high frequency coefficients of the discrete Fourier transform of the parameters $\mathbf{P}$, i.e. by minimising ζ^2 (Eq.4 below) at the same time as χ^2 (Eq.2).

$$\zeta^2 = tr\left([\mathbf{S}_{l_0}\cdot\mathbf{T}\cdot\mathbf{P}]^{\rm T}\cdot[\mathbf{S}_{l_0}\cdot\mathbf{T}\cdot\mathbf{P}]\right) \quad (4)$$

where $\mathbf{T}$ is the matrix of the discrete Fourier transform and $\mathbf{S}_{l_0}$ the high frequency filter that cancels the coefficients of the Fourier transform corresponding to a length (in the parameter space) greater than l_0.

Actually, the overall fit with the regularisation constraint is done by using a Lagrange parameter f_0 and minimising the following quantity,

$$Q = \chi^2 + f_0\,\zeta^2 \quad (5)$$

The parameter f_0 controls the relative strength of the regularisation over the χ^2 fit of the data. If f_0 is too small, then only χ^2 is minimized and the data will be over-fitted. On the contrary, if f_0 is to large, the minimisation is done only for ζ^2 giving a very smooth solution that does not fit the data. Thus, f_0 is chosen to obtained a χ^2 value approximately equal to 1.

In the worst case, since there are more parameters ($n*(m+1)$) than data points ($n*m$), the problem is underestimated. Nevertheless, the regularisation introduces a constraint that diminishes the real number of free parameters. Moreover, in practice, most of the profiles we use here are free of blending and, in that case, we impose a zero optical depth for the intervening absorption.

Once the different profiles have been fitted, we compute the mean ratios between the most important elements in order to analyse the possible variations of the ratios along the profile.

4. Results on individual objects

Several of the systems in the sample are spread over more than 200 km s^{-1}. The absorption profiles are often clearly structured in several well detached clumps with no or very few absorption inbetween. To investigate whether the properties differ from one clump to the other, we have performed the analysis on each of the clumps. Indeed, it is reasonable to believe that different part of the DLAs could have different characteristics (e.g. Haehnelt et al. 1998) Column densities of several species, integrated over the system, are given for each system in Table 3. Abundance ratios relative to solar are defined as [X/Y] = $\log[N({\rm X})/N({\rm Y})]$ - $\log[N({\rm X})/N({\rm Y})]_\odot$ adopting solar abundances from Savage & Sembach (1996). We compute the quantity [X/Y] in each pixel and its average ($\overline{[X/Y]}$) over each subclump. Results are given in Tables 3 to 7. Each subclump is referred to by the velocity range over which it is spread relative to the main redshift of the system. $\overline{[X/Y]}$, averaged over this velocity range, is given for each ratio. In each row, the number next to $\overline{[X/Y]}$ is the error on the mean ratio ($\sigma = \sqrt{\sum_{i=1}^{n}\sigma_i^2/n}$), and the second number (in italics) is the scatter of [X/Y] around the mean calculated over the subclump.

4.1. Q 0013−004

As mentioned in Section 4.1, the absorption system found in the line of sight of Q 0013−004 at $z_{\rm abs} = 1.973$ shows a complex multicomponent structure. Besides the fact that the system is composed by a DLA at $z_{\rm abs} = 1.96753$ and a sub-DLA at $z_{\rm abs} = 1.9733$ (Petitjean et al. 2002), the low-ionization absorptions span about 1000 km s^{-1} and the system exhibits four molecular components at ~ -615, -480, 0 and 85 km s^{-1} relative to the central redshift.

Figure 7, illustrates this complexity. The apparent column density per velocity bin, referred to solar values is plotted for Fe II, S II and Si II. All have complex but remarquably similar profiles. The other panels represent the pixel-by-pixel ratio [Fe/S].

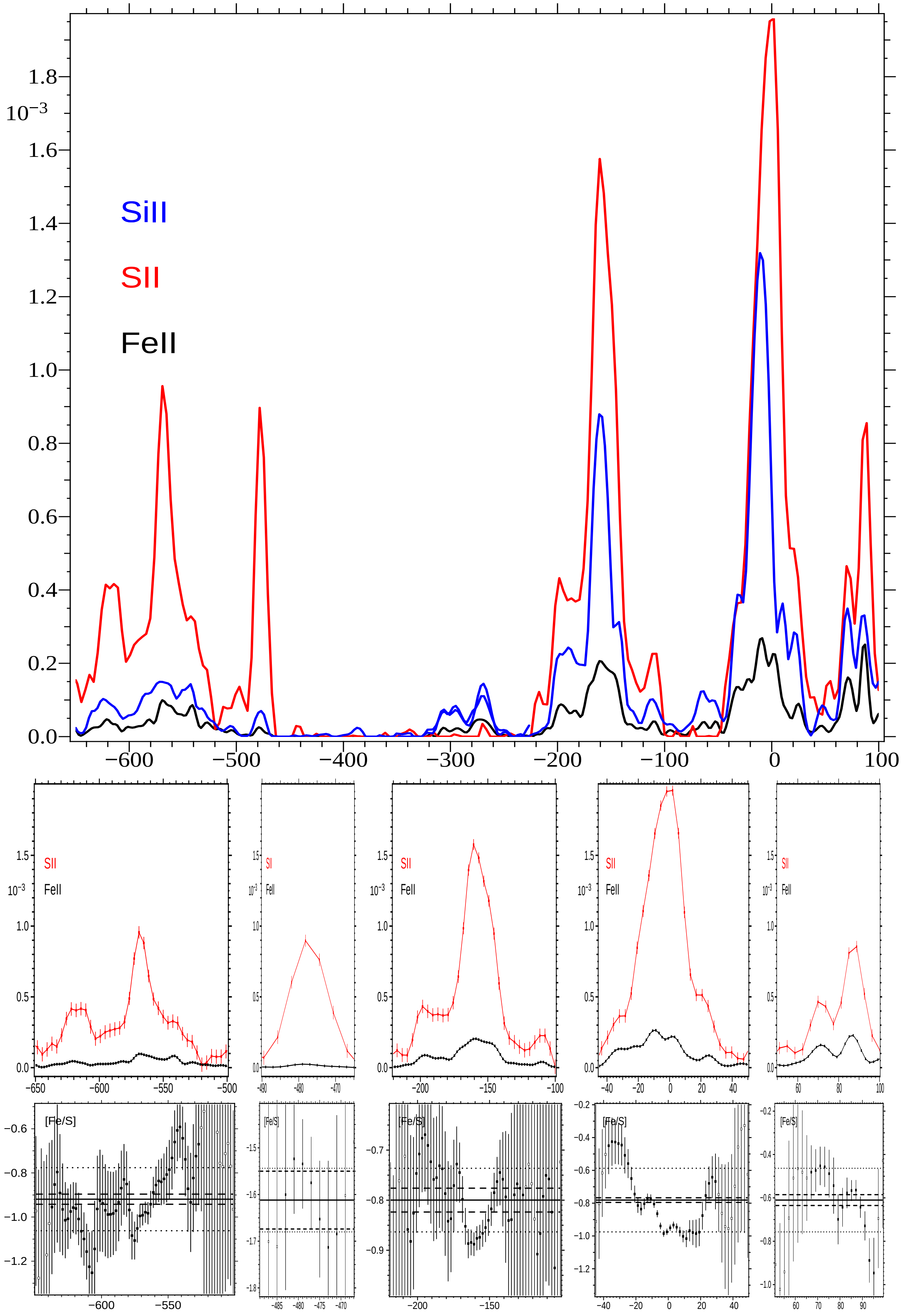

Fig. 7. Top panels show the optical depth profiles in the $z_{\rm abs} = 1.973$ DLA toward Q 0013−004. The apparent column density per velocity bin -$N(X, dv)$- is represented on a velocity scale, with $v = 0$ km s^{-1} centered at $z_{\rm abs} = 1.973$. The lower panels show the ratio [Fe/S] computed for each pixel. Points with too big errors are rejected to compute the mean, represented here as empty squares, while valid points are filled. The mean value is plotted as a solid line. Dashed lines represent the $\pm\sigma$ level and the dotted line the typical scatter of the points. H$_2$ is detected in four components at $\sim$−615, −480, 0 and 85 km s^{-1}.

	Q 0013−004			
	[-650,-500]	[-220,-100]	[-45,50]	[50,100]
$[Fe/S]$	$-0.92 \pm 0.02 \pm \mathit{0.15}$	$-0.80 \pm 0.02 \pm \mathit{0.07}$	$-0.78 \pm 0.01 \pm \mathit{0.20}$	$-0.61 \pm 0.02 \pm \mathit{0.16}$
$[Si/S]$	$-0.55 \pm 0.03 \pm \mathit{0.13}$	$-0.31 \pm 0.08 \pm \mathit{0.08}$	$-0.24 \pm 0.06 \pm \mathit{0.22}$	$-0.24 \pm 0.06 \pm \mathit{0.15}$
$[Ni/S]$	$-0.48 \pm 0.10 \pm \mathit{0.23}$	—	$-0.61 \pm 0.06 \pm \mathit{0.18}$	$-0.36 \pm 0.09 \pm \mathit{0.21}$
$[Fe/Si]$	$-0.35 \pm 0.02 \pm \mathit{0.12}$	$-0.49 \pm 0.06 \pm \mathit{0.10}$	$-0.55 \pm 0.01 \pm \mathit{0.16}$	$-0.34 \pm 0.04 \pm \mathit{0.12}$
$[Fe/Ni]$	$-0.42 \pm 0.07 \pm \mathit{0.20}$	—	$-0.18 \pm 0.05 \pm \mathit{0.12}$	$-0.18 \pm 0.08 \pm \mathit{0.16}$

Table 4. Abundance ratios for the system observed at $z_{\rm abs} = 1.973$ in the line of sight of Q 0013−004. We have decomposed the system in eight subclumps. The table corresponds to the four clumps without H_2. Values for the peculiar regions where H_2 is detected are given in Table 5.

	Q0013-004			
	[-630,-605]	[-490,-465]	[-15,15]	[76,95]
$[Fe/S]$	$\mathbf{-1.04 \pm 0.05}$	$\mathbf{-1.60 \pm 0.06}$	$\mathbf{-0.90 \pm 0.01}$	$\mathbf{-0.64 \pm 0.03}$
$[Si/S]$	$\mathbf{-0.62 \pm 0.06}$	$\mathbf{-1.14 \pm 0.26}$	$\mathbf{-0.33 \pm 0.01}$	$\mathbf{-0.34 \pm 0.04}$
$[Ni/S]$	$\mathbf{-0.75 \pm 0.25}$	–	$\mathbf{-0.73 \pm 0.05}$	$\mathbf{-0.50 \pm 0.10}$
$[Fe/Si]$	$\mathbf{-0.42 \pm 0.03}$	$\mathbf{-0.46 \pm 0.26}$	$\mathbf{-0.58 \pm 0.01}$	$\mathbf{-0.30 \pm 0.03}$
$[Fe/Ni]$	$\mathbf{-0.29 \pm 0.25}$	$\mathbf{-0.27 \pm 0.64}$	$\mathbf{-0.17 \pm 0.05}$	$\mathbf{-0.14 \pm 0.10}$

Table 5. Abundance ratios for the system observed at $z_{\rm abs} = 1.973$ in the line of sight of Q 0013−004. We have decomposed the system in eight subclumps. The table corresponds to the four clumps with H_2. Values for other subclumps of the system are given in Table 4.

The mean values (see Table 4) are smaller than in other systems but are again quite similar from one sub-clump to the other. Within a peculiar sub-clump, scatter is small, of the order of 0.2 dex. In the components where H_2 is detected, the depletion factor is of the order of [Fe/S] = −1, therefore slightly smaller but not much than in the overall system, except in the component at −480 km s^{-1} which is the only region in DLAs known todate where depletion is of the same order as in the cold gas of the Galactic disk.

4.2. Q 0405−443

We have analysed the systems at $z_{\rm abs} = 2.549$ and $z_{\rm abs} = 2.495$ toward Q 0405−443.

In the latter system, molecular hydrogen has been detected with a column density, $\log N(H_2) = 18.16$ (Ledoux et al., 2003). Relatively narrow, low-ionisation transitions span about 70 km s^{-1}. It is apparent from Figure 9 that there are some inhomogeneities inside the system and there is more depletion (by about a factor of two) in the two components where H_2 is detected at $v \sim -8$ and −24 km s^{-1}. Note that the depletion is larger in these components but not by a large amount and definitively not as in cold gas of the Galaxy disk. The scatter of the pixel values is much larger than the errors for all element ratios (see Table 6). The overall depletion pattern is again similar to that of warm gas of the halo, with a slight enhancement of Cr.

The system at $z_{\rm abs} = 2.549$, presented in Figure 8, shows absorptions spread over ∼ −120 km s^{-1}, and is well structured in three subclumps. From both Figure 8 and Table 6 we can see that the three subclumps at velocities [-30,20], [40, 60] and [60, 90] are quite homogeneous but have slighly different mean depletion factors, [Fe/S] = −0.26, −0.08 and −0.33 respectively. However again, the differences are smaller than 0.2 dex. In addition, the depletion values are close to those of the $z_{\rm abs} = 2.595$ system, that is located ∼ −3000 km s^{-1} away.

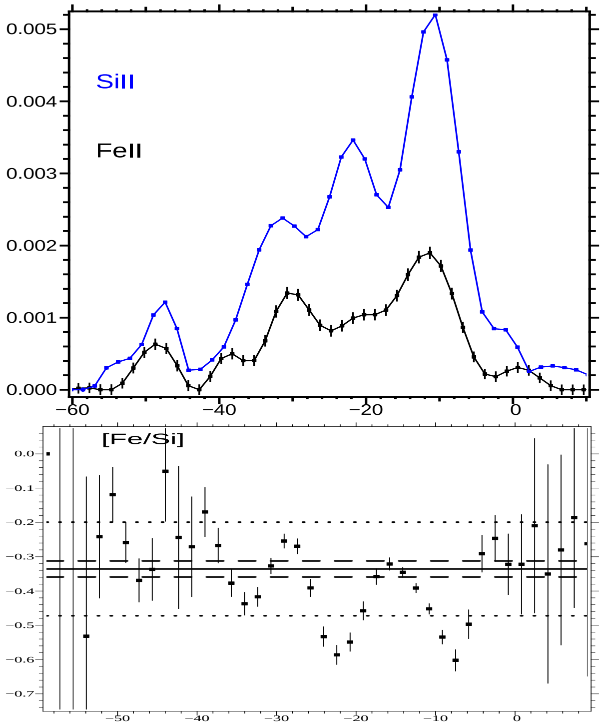

Fig. 9. Top panel shows the optical depth profiles in the $z_{\rm abs} = 2.495$ DLA toward Q 0405−443. The apparent column density per velocity bin -$N(X, dv)$- is represented on a velocity scale, with $v = 0$ km s^{-1} centered at $z_{\rm abs} = 2.495$. The lower panels show the ratio [Fe/Si] computed for each pixel. The mean value is plotted as a solid line. Dashed lines represent the $\pm\sigma$ level and the dotted line the typical scatter of the points. This DLA has two molecular components at $v \sim -24$ and ~ -11 km s^{-1}.

4.3. Q 0528−250

The system is spread over more than 350 km s^{-1} and exhibit two molecular components located at ∼ 0 km s^{-1}.

We observe in Figure 10 that the internal structure is complex with many components. Note that the profiles of

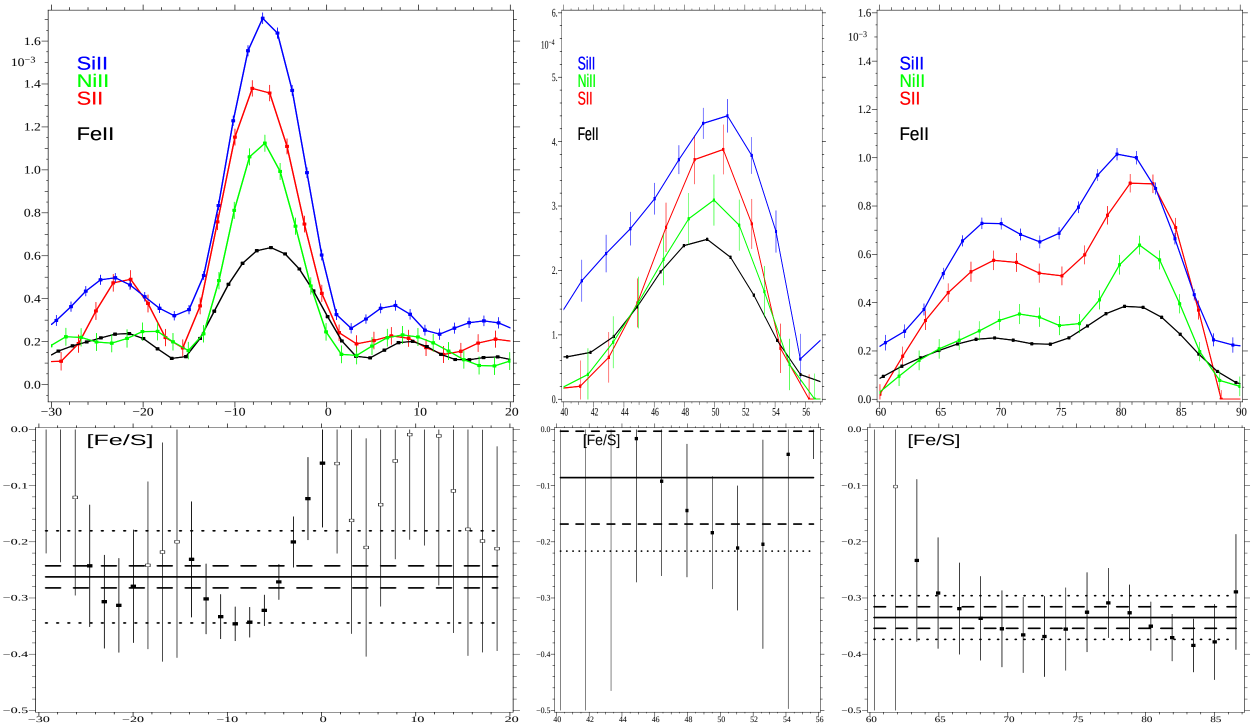

Fig. 8. Top panel shows the optical depth profiles in the $z_{\rm abs} = 2.549$ DLA toward Q 0405−443. The apparent column density per velocity bin -$N(X, dv)$- is represented on a velocity scale for Si, Ni, S and Fe; with $v = 0$ km s^{-1} centered at $z_{\rm abs} = 2.549$. The lower panels show the ratio [Fe/S] computed for each pixel. The mean value is plotted as a solid line. Dashed lines represent the $\pm\sigma$ level and the dotted line the typical scatter of the points.

	Q 0405−443 $z_{\rm abs} = 2.495$			Q 0405−443 $z_{\rm abs} = 2.549$		
	[-60,10]	**[-30,-14]**	**[-17,-2]**	[-30,20]	[40,60]	[60,90]
$[Fe/S]$	$-0.27 \pm 0.02 \pm \mathit{0.13}$	$\mathbf{-0.34 \pm 0.01}$	$\mathbf{-0.37 \pm 0.01}$	$-0.26 \pm 0.02 \pm \mathit{0.08}$	$-0.08 \pm 0.08 \pm \mathit{0.13}$	$-0.33 \pm 0.02 \pm \mathit{0.04}$
$[Si/S]$	$0.07 \pm 0.01 \pm \mathit{0.08}$	$\mathbf{0.03 \pm 0.01}$	$\mathbf{0.07 \pm 0.01}$	$0.07 \pm 0.02 \pm \mathit{0.05}$	$0.17 \pm 0.10 \pm \mathit{0.12}$	$0.09 \pm 0.02 \pm \mathit{0.07}$
$[Ni/S]$	$-0.29 \pm 0.02 \pm \mathit{0.15}$	$\mathbf{-0.37 \pm 0.01}$	$\mathbf{-0.38 \pm 0.01}$	$-0.17 \pm 0.04 \pm \mathit{0.11}$	$-0.05 \pm 0.10 \pm \mathit{0.04}$	$-0.23 \pm 0.04 \pm \mathit{0.05}$
$[Cr/S]$	$-0.16 \pm 0.03 \pm \mathit{0.17}$	$\mathbf{-0.16 \pm 0.03}$	$\mathbf{-0.23 \pm 0.04}$	$0.05 \pm 0.06 \pm \mathit{0.10}$	$0.00 \pm 0.26 \pm \mathit{0.18}$	$-0.18 \pm 0.08 \pm \mathit{0.10}$
$[Fe/Si]$	$-0.34 \pm 0.02 \pm \mathit{0.13}$	$\mathbf{-0.37 \pm 0.01}$	$\mathbf{-0.44 \pm 0.01}$	$-0.35 \pm 0.01 \pm \mathit{0.04}$	$-0.30 \pm 0.03 \pm \mathit{0.07}$	$-0.43 \pm 0.01 \pm \mathit{0.04}$
$[Fe/Ni]$	$0.00 \pm 0.01 \pm \mathit{0.08}$	$\mathbf{0.03 \pm 0.01}$	$\mathbf{0.01 \pm 0.01}$	$-0.09 \pm 0.03 \pm \mathit{0.09}$	$-0.05 \pm 0.09 \pm \mathit{0.05}$	$-0.11 \pm 0.03 \pm \mathit{0.07}$
$[Fe/Cr]$	$-0.19 \pm 0.03 \pm \mathit{0.06}$	$\mathbf{-0.18 \pm 0.03}$	$\mathbf{-0.14 \pm 0.04}$	—	—	—

Table 6. Abundance ratios for the systems observed in the lines of sight of Q 0405−443. For the $z_{\rm abs} = 2.595$ system. We have singled out the H_2 components and numbers are given in bold.

Fe and S follow each other remarkably well over most of the profile. The pixel-by-pixel analysis give similar results for each of the subclumps, suggesting that once again the mixing of heavy element must have been very efficient in this system (see Table 7).

The central part at [0, 20] has a larger depletion coefficient, down to [Fe/S] = −0.55, when the rest of the system has [Fe/S] ∼ −0.3. This is the place where, again, H$_2$ is detected. Eventhough the depletion factor is larger in this component, it is much smaller than in cold gas of the Galactic ISM. The overall depletion pattern in the system is very close to what is observed in the Galactic halo (see Table 7).

4.4. Q 1037−270

Figure 11 shows the column density per pixel along the profile for different species, including Fe II, Si II, S II, and Ni II. All species follow the same pattern and their ratios remain fairly constant all over the profile.

We consider two subclumps for $-10 < v < 30$ and $40 < v < 60$ km s^{-1} (see Table 8). There is essentially no difference between the two subclumps. Note that the scatter is comparable to or smaller than the errors (for the first [-10,30] subclump, $\sigma_{\rm e} = 0.04$, $\sigma_{\rm s} = 0.07$ and for the second, [40,60], $\sigma_{\rm e}$[Fe/S] $= 0.07$ and $\sigma_{\rm s} = 0.02$).

This system is therefore fairly homogeneous within 0.1 dex and the abundance pattern similar to what is observed in warm gas of the Galactic halo.

4.5. Q 1157+014

This system is spread over about 100 km s^{-1} and has no associated molecules detected. We consider only one clump. Pixel analysis is shown in Fig. 12. Unfortunately sufur transitions are blended with intervening absorptions

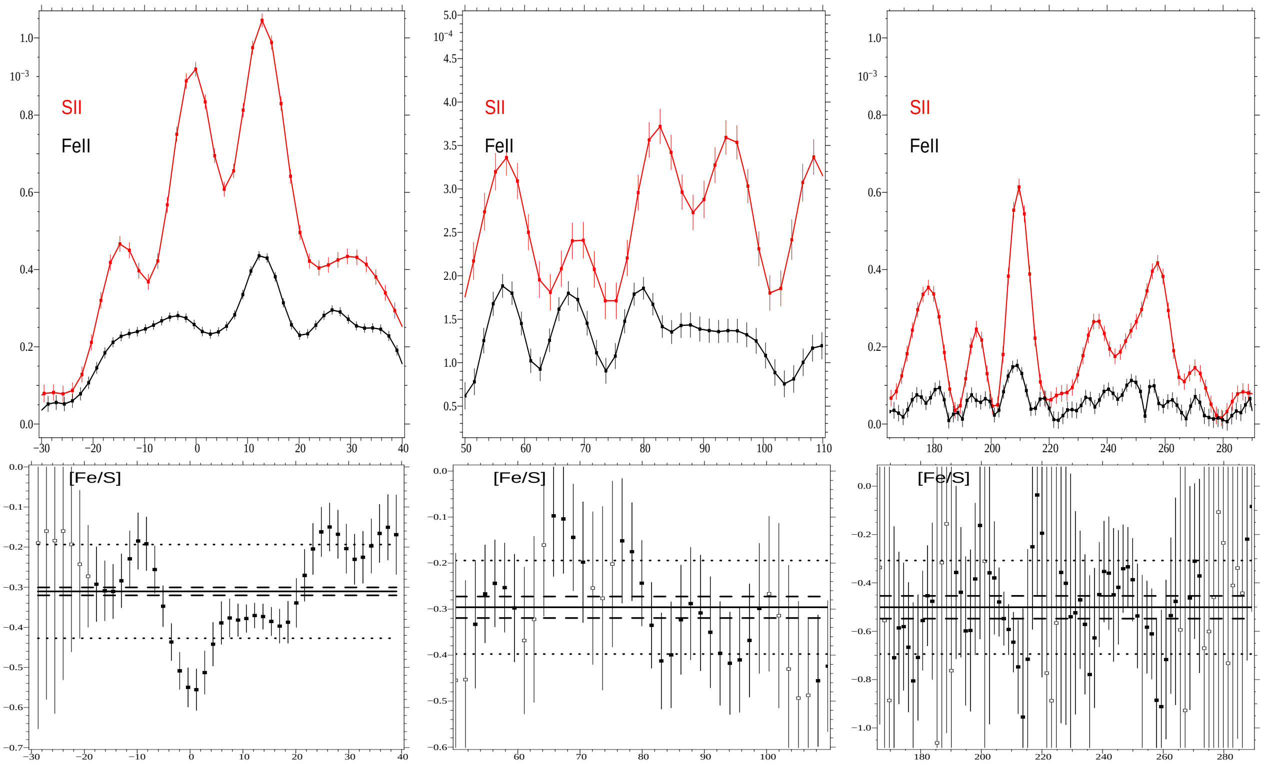

Fig. 10. Top panel shows the optical depth profiles in the $z_{\rm abs} = 2.811$ DLA toward Q 0528−250. The apparent column density per velocity bin -$N(X, dv)$- is represented on a velocity scale, with $v = 0$ km s^{-1} centered at $z_{\rm abs} = 2.811$. The lower panels show the ratio [Fe/S] computed for each pixel. The mean value is plotted as a solid line. Dashed lines represent the $\pm\sigma$ level and the dotted line the typical scatter of the points. H_2 is detected in two components at ~ 0 km s^{-1}.

	Q 0528−250			
	[-30,40]	**[-8,8]**	[50,110]	[165,290]
$[Fe/S]$	$-0.31 \pm 0.01 \pm \mathit{0.11}$	$\mathbf{-0.44 \pm 0.01}$	$-0.29 \pm 0.02 \pm \mathit{0.10}$	$-0.50 \pm 0.05 \pm \mathit{0.20}$
$[Si/S]$	$0.27 \pm 0.01 \pm \mathit{0.10}$	$\mathbf{0.18 \pm 0.01}$	$0.14 \pm 0.02 \pm \mathit{0.06}$	$-0.02 \pm 0.02 \pm \mathit{0.12}$
$[Ni/S]$	$-0.25 \pm 0.01 \pm \mathit{0.11}$	$\mathbf{-0.38 \pm 0.02}$	$-0.27 \pm 0.04 \pm \mathit{0.06}$	$-0.49 \pm 0.06 \pm \mathit{0.17}$
$[Fe/Si]$	$-0.58 \pm 0.01 \pm \mathit{0.09}$	$\mathbf{-0.63 \pm 0.01}$	$-0.45 \pm 0.02 \pm \mathit{0.07}$	$-0.54 \pm 0.04 \pm \mathit{0.14}$
$[Fe/Ni]$	$-0.07 \pm 0.01 \pm \mathit{0.06}$	$\mathbf{-0.07 \pm 0.02}$	$-0.02 \pm 0.04 \pm \mathit{0.05}$	$-0.09 \pm 0.07 \pm \mathit{0.17}$

Table 7. Abundance ratios for the system observed at $z_{\rm abs} = 2.811$ in the line of sight of Q 0528−250. The molecular component at $v \sim 0$ km s^{-1} has been isolated from the rest of the absorption (second column, in bold).

and we use zinc as the non-depleted species reference instead.

The system has a low mean metallicity, [Zn/H] $= -1.40$ (see Table 1), and shows a very similar depletion pattern as the halo of the galaxy for every element analysed.

Pixel analysis is shown in Fig. 12. It can be seen that depletion is higher, [Fe/Zn] ~ -0.65, in the strongest absorption component. It should be noticed that 21 cm absorption has been reported by Kanekar & Chengalur (2003) at this velocity (~ -28 km s^{-1}), revealing dense gas. The difference in depletion between the strongest subcomponent (at -28 km s^{-1}) and the gas at $v \sim -40$ km s^{-1} is significant (about a factor of two is larger than 3σ). This is clearly a sign of more depletion in the dense gas producing the 21 cm absorption. The overall scatter is only about 0.12 dex (see Table 8). This is fairly small compared to what is observed through the ISM of our Galaxy (Welty et al., 1999). In addition, Ni and Fe follow each other very well.

5. Discussion

5.1. Relative Abundance Ratios

As described in detail in the previous Sections, relative abundance ratios for each sub-clump considered in the six systems analysed in this work are given in Tables 8 to 5. Results are summarized in Fig. 13. It is apparent that, within each subsystem, large departures from the mean ratio are rare: the scatter is small if we take into account the observational and fitting uncertainties. Moreover, when we compare depletion values from one sub-clump to another in the same system, differences are small. Only for some molecular components a distinct depletion pattern is observed.

This is remarquably summarized by Fig. 14 where we plot the [Fe/S] ratio versus the [Si/S] ratio in all sub-

	Q 1157+014		Q 1037−270	
	[−70,15]		[−10,30]	[40,60]
$[Fe/Zn]$	$-0.43 \pm 0.02 \pm \mathit{0.12}$	$[Fe/S]$	$-0.34 \pm 0.04 \pm \mathit{0.07}$	$-0.22 \pm 0.07 \pm \mathit{0.02}$
$[Si/Zn]$	$0.05 \pm 0.02 \pm \mathit{0.05}$	$[Si/S]$	$0.17 \pm 0.03 \pm \mathit{0.03}$	$0.16 \pm 0.05 \pm \mathit{0.04}$
$[Ni/Zn]$	$-0.43 \pm 0.03 \pm \mathit{0.12}$	$[Ni/S]$	$-0.01 \pm 0.04 \pm \mathit{0.04}$	$0.00 \pm 0.07 \pm \mathit{0.05}$
$[Cr/Zn]$	$-0.29 \pm 0.02 \pm \mathit{0.12}$	$[Cr/S]$	—	—
$[Fe/Si]$	$-0.49 \pm 0.01 \pm \mathit{0.09}$	$[Fe/Si]$	$-0.51 \pm 0.03 \pm \mathit{0.06}$	$-0.38 \pm 0.05 \pm \mathit{0.05}$
$[Fe/Ni]$	$0.00 \pm 0.02 \pm \mathit{0.05}$	$[Fe/Ni]$	$-0.33 \pm 0.04 \pm \mathit{0.06}$	$-0.22 \pm 0.06 \pm \mathit{0.06}$
$[Fe/Cr]$	$-0.14 \pm 0.02 \pm \mathit{0.06}$	$[Fe/Cr]$	—	—
$[Fe/Zn]$	$-0.43 \pm 0.02 \pm \mathit{0.12}$	$[Fe/Zn]$	—	—

Table 8. Abundance ratios for the systems observed along the lines of sight to Q 1157+014 and Q 1037−270. For each range of velocities we compute the mean ratio, its error $\sigma = \sqrt{\sum_{i=1}^{n} \sigma_i^2/n}$, as well as the standard deviation around the mean, as an indicator of the inhomogeneity through the subclump.

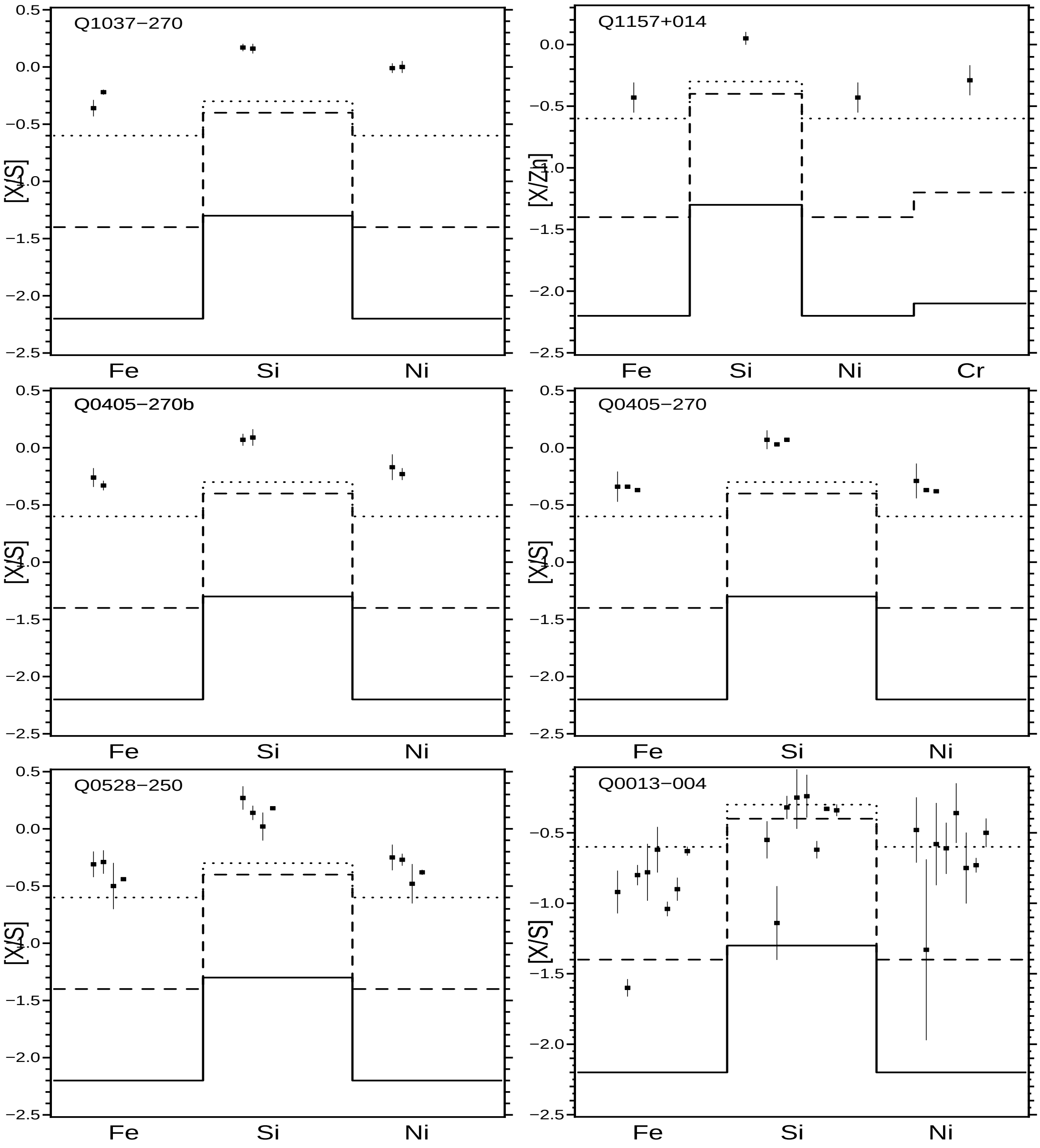

Fig. 13. Depletion of heavy elements relative to Sulfur (except for Q 1157+014, where Zinc is used instead) in the different subclumps of the six DLA systems studied here. Filled squars represent the different sub-systems considered (see Tables 8 to 5). Error bars correspond to typical scatter for each sub-system. The histograms show the observed values in the cold (solid line) or warm (dashed line) disc clouds and in halo clouds (dotted line) of the Galaxy.

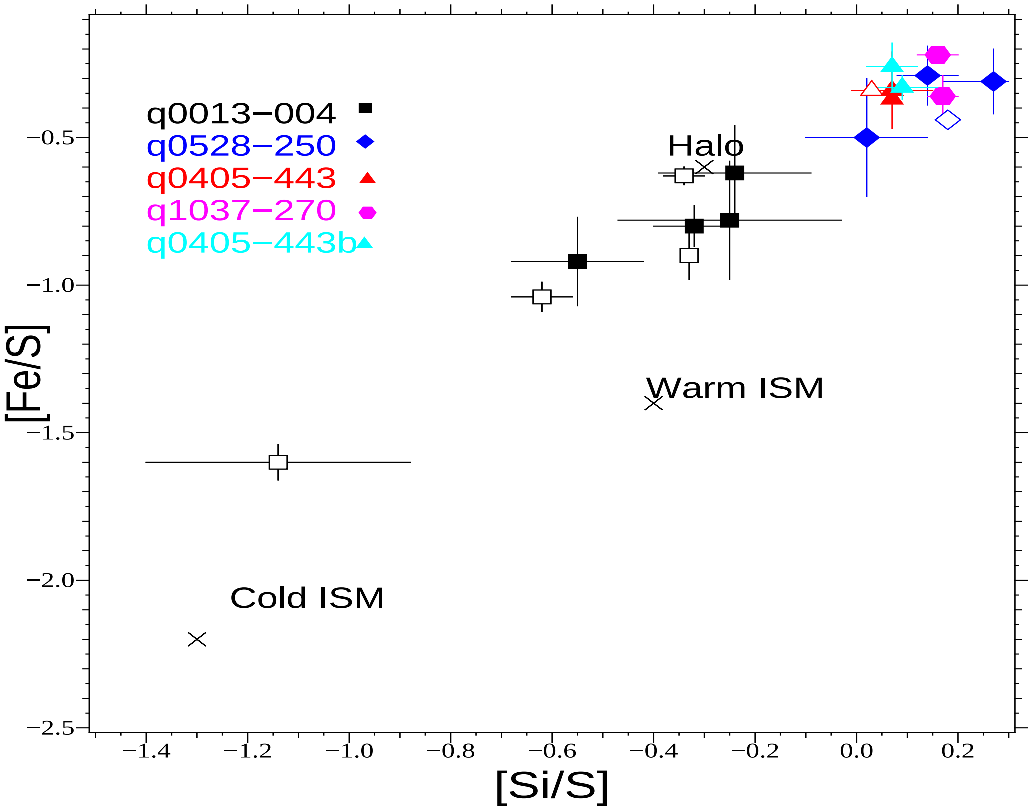

Fig. 14. [Fe/S] vs [Si/S] for all the subclumps analysed in this paper. Different symbols represent different DLA: squares for Q 0013−004, diamonds for Q 0528−250, triangles for Q 0405−443 and circles for Q 1037−270. Open symbols are used to distinguish subclumps where H_2 is detected. Otherwise symbols are filled. We have also indicated the typical [Fe/S] vs [Si/S] values observed in the cold, warm ISM and halo of our Galaxy from Welty et al. (1999).

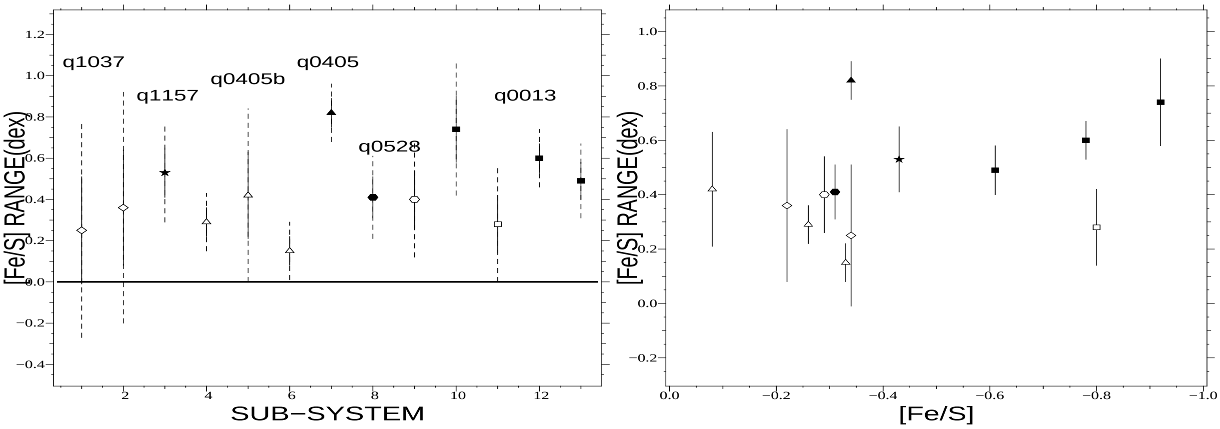

Fig. 15. The two panels summarize the inhomogeneity amplitude observed in the subsystems. The y-axis represents the maximum deviation of $[Fe/S] \pm 2\sigma$ in each subclumps. Subsystems with molecules are respresented with filled symbols.

clumps. The same symbol is used for different clumps in the same system. Filled symbols are used for clumps where H_2 is detected and empty symbols otherwise. First, as already emphasized by Petitjean et al. (2002) and Ledoux et al. (2002b), the sequence seen in the Figure is a dust-depletion sequence. Indeed, there is a correlation between the two quantities which is expected if the depletion is due to the presence of dust. Secondly, the values measured in different clumps of the same system are gathered at the same place in the Figure. The only exception is the H_2 component at −480 km s^{-1} in Q 0013−004 (see above). Thirdly, most of the depletion pattern is similar to that of the gas observed in the Galactic halo. Finally it seems that silicon is overabundant by about 0.2 dex even relative to sulfur. In all this however it must be reminded that we do not have access to the absolute metallicity in the subclumps because we are not able to disentangle the H I absorptions of the different clumps.

In the left handside panel of Fig. 15, we plot the scatter, measured as σ, of the ratio [Fe/S] in all the subclumps

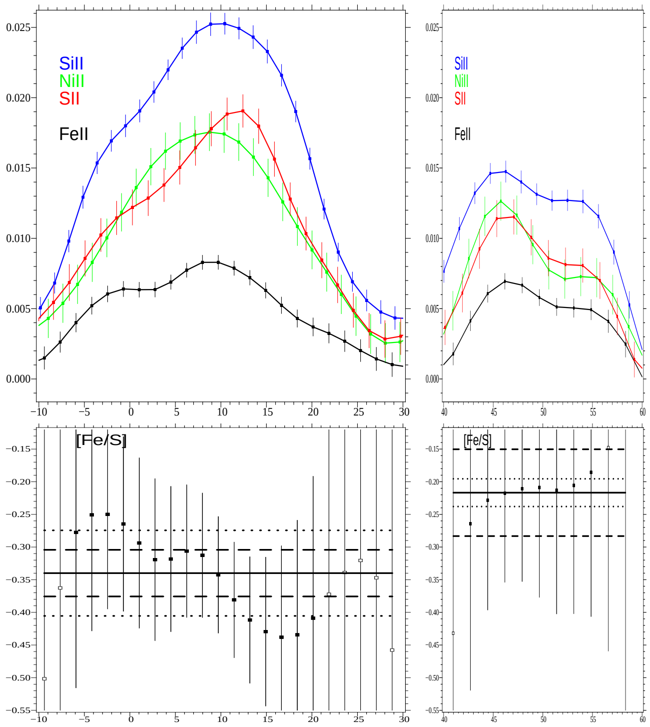

Fig. 11. Top panel shows the optical depth profiles in the $z_{\rm abs} = 2.139$ DLA towards Q 1037−270. The apparent column density per velocity bin -$N(X, dv)$- is represented on a velocity scale, with $v = 0$ km s^{-1} centered at $z_{\rm abs} = 2.139$. The lower panel shows the ratio [Fe/S] computed for each pixel. The mean value is plotted as a solid line. Dashed lines represent the $\pm\sigma$ level and the dotted line the typical scatter of the points.

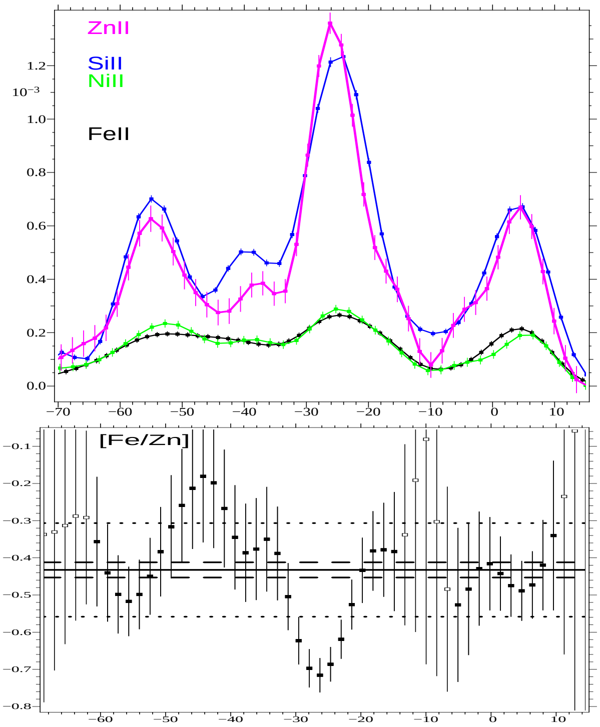

Fig. 12. Top panel shows the optical depth profiles in the $z_{\rm abs} = 1.944$ DLA towards Q 1157+014. The apparent column density per velocity bin -$N(X, dv)$- is represented on a velocity scale for Zn, Si, Ni and Fe species, with $v = 0$ km s^{-1} centered at $z_{\rm abs} = 1.944$. The lower panel shows the ratios [Fe/Zn] computed for each pixel. The mean value is plotted as a solid line. Dashed lines represent the $\pm\sigma$ level and the dotted line the typical scatter of the points.

considered. Filled symbols are for subclumps where H_2 is detected. The mean value of σ over the subclumps is 0.3. This means that inhomogeneities are less than a factor of 2. Only a few subclumps where H_2 is detected have larger σ. This is expected because we have seen that depletion is larger over the specific small velocity ranges over which H_2 is detected.

In the right handside panel of Fig. 15, we plot the different scatter values for each subclump as a function of the total [Fe/S] ratio. This Figure confirms that (i) larger [Fe/S] ratios are observed in subclumps where H_2 is detected (there is one exception in a subclump of Q 0013−0004) and (ii) the scatter is larger for subclumps where H_2 is detected.

5.2. The role of Molecules H_2

Ledoux et al. (2003) have searched systematically for molecular hydrogen in high redshift DLAs, with ∼20% detection rate. over the whole sample. The observed molecular fraction is often much smaller than in the ISM of the Galactic disk (Rachford et al. 2002) and is closer to what is observed in the halo (Tumlinson et al. 2002). Here, we confirm what was already noticed by Ledoux et al. (2002b) and Petitjean et al. (2002) that, although the presence of molecules reveals sometimes gas with larger depletion into dust grains than average, this is not always the case. In most of the systems, the depletion factor is only a factor of two larger in the components with H_2 compared to the overall system. There are a few exceptions, the most noticeable beeing the molecular component at −480 km s^{-1} toward Q 0013−014 in which depletion is as large as in the cold gas of the Galactic disk.

Acknowledgements. RS and PPJ gratefully acknowledge support from the Indo-French Center for the Promotion of Advanced Research (Centre Franco-Indien pour la Promotion de la Recherche Avancée) under contract No.3004-3.

References

Briggs, F.H., Turnshek, D.A., & Wolfe, A.M. 1984, ApJ, 287, 549
Centurion, M., Bonifacio, P., Molaro, P., Vladilo, G. 2000 ApJ536, 540
D'Odorico, S., Cristiani, S. Dekker, H. et al 2000, Proc.SPIE Vol.4005, p.121
Ge, J. & Bechtold, J. 1997, ApJ, 477, L73
Haehnelt, M. G., Steinmetz, M., & Rauch, M. 1998, ApJ, 495, 647
Hou, J. L., Boissier, S., & Prantzos, N. 2001, A&A, 370, 23

Kanekar, N., Chengalur, J. N., 2003, A&A, 399, 857

Ledoux, C., Petitjean, P., Bergeron, J., Wampler, E. J., & Srianand, R. 1998, A&A, 337, 51

Ledoux, C., Bergeron, J., Petitjean, P. 2002 A&A385, 802

Ledoux, C., Srianand, R., Petitjean, P. 2002 A&A392, 781

Ledoux, C., Petitjean, P., Srianand, R. 2003 MNRAS, 346, 209

Lespine, Y., & Petitjean, P. 1997, A&A, 317, 416

Lopez, S., Maza, J., Masegosa, J., Marquez, I. 2001, A&A, 366, 387

Lopez, S., Reimers, D., D'Odorico S., & Prochaska, J. X. 2002, A&A, 385, 778

Levshakov, S. A. & Varshalovich, D. A. 1985, MNRAS, 212, 517

Lu, L., Sargent, W. L. W., Barlow, T. A., Churchill, C. W., & Vogt, S. S. 1996, ApJS, 107, 475

McWilliam, A. 1997 ARA&A, 35, 503

Petitjean, P., Srianand, R. and Ledoux, C. 2002 MNRAS, 332, 383

Pettini, M., Smith, L. J., Hunstead, R. W., & King, D. L. 1994, ApJ, 426, 79

Prochaska, J.X. 2003, ApJ, 582, 49

Prochaska, J. X. & Wolfe, A. M. 1997, ApJ, 487, 73

Prochaska, J. X. & Wolfe, A. M. 1999, ApJS, 121, 369

Prochaska, J. X. & Wolfe, A. M. 2002, ApJ, 566, 68

Rachford, B. L., et al. 2002, ApJ, 577, 221

Savage, B. D. & Sembach, K. R. 1991, ApJ, 379, 245

Savage, B. D. & Sembach, K. R. 1996, ARA&A, 34, 279

Songaila, A. & Cowie, L. L. 1996, AJ, 112, 335

Srianand, R., & Petitjean, P. 1998, A&A, 335, 33

Srianand, R., & Petitjean, P. 2001, A&A, 373, 816

Storrie-Lombardi, L. J. & Wolfe, A. M. 2000, ApJ, 543, 552

Tinsley, B.M. 1979 ApJ, 229, 1046

Tumlinson, J., Shull, J. M., Rachford, B. L., et al. 2002, ApJ, 248, 460

Viegas, S. M. 1995, MNRAS, 276, 268

Welty, D. E., Hobbs, L. M., Lauroesch,J. T et al. 1999, ApJS, 124, 465

Welty, D. E., Lauroesch, J. T., Blades, J. C., Hobbs, L. M., & York, D. G. 2001, ApJ, 554, L75

Wolfe, A. M., Turnshek, D. A., Smith, H. E., Cohen, R. D., 1986, ApJS, 61, 249

Species	$N(\mathrm{cm}^{-2})$	[X/S]	[X/Fe]
Q 0013−004	$z_{\rm abs} = 1.973$		
FeII	$7.55 \pm 0.01 \times 10^{14}$	-0.78 ± 0.03	0.00 ± 0.00
SII	$2.64 \pm 0.08 \times 10^{15}$	0.00 ± 0.00	0.78 ± 0.03
SiII	$2.72 \pm 0.20 \times 10^{15}$	-0.27 ± 0.08	0.51 ± 0.07
ZnII	$7.30 \pm 1.12 \times 10^{12}$	0.06 ± 0.15	0.84 ± 0.15
NiII	$7.57 \pm 0.72 \times 10^{13}$	-0.52 ± 0.05	0.26 ± 0.04
Q 0405−443	$z_{\rm abs} = 2.549$		
FeII	$1.05 \pm 0.01 \times 10^{15}$	-0.53 ± 0.04	0.00 ± 0.00
SII	$2.03 \pm 0.07 \times 10^{15}$	0.00 ± 0.00	0.53 ± 0.14
SiII	$2.38 \pm 0.32 \times 10^{15}$	-0.21 ± 0.15	0.32 ± 0.14
CrII	$2.46 \pm 0.76 \times 10^{13}$	-0.33 ± 0.31	0.20 ± 0.31
NiII	$7.05 \pm 0.96 \times 10^{13}$	-0.44 ± 0.14	0.09 ± 0.14
Q 0405−443	$z_{\rm abs} = 2.595$		
FeII	$1.30 \pm 0.13 \times 10^{15}$	-0.37 ± 0.10	0.00 ± 0.00
SII	$1.75 \pm 0.04 \times 10^{15}$	0.00 ± 0.00	0.37 ± 0.10
SiII	$3.52 \pm 0.07 \times 10^{15}$	0.03 ± 0.03	0.40 ± 0.10
CrII	$2.23 \pm 0.07 \times 10^{13}$	-0.30 ± 0.04	0.06 ± 0.10
NiII	$6.92 \pm 0.08 \times 10^{13}$	-0.38 ± 0.02	-0.02 ± 0.10
Q 0528−250	$z_{\rm abs} = 2.811$		
FeII	$2.60 \pm 0.03 \times 10^{15}$	-0.37 ± 0.01	0.00 ± 0.00
SII	$3.49 \pm 0.02 \times 10^{15}$	0.00 ± 0.00	0.37 ± 0.01
SiII	$1.01 \pm 0.05 \times 10^{16}$	0.18 ± 0.05	0.55 ± 0.05
ZnII	$1.27 \pm 0.26 \times 10^{13}$	0.18 ± 0.21	0.55 ± 0.21
CrII	$7.18 \pm 1.45 \times 10^{13}$	-0.10 ± 0.20	0.17 ± 0.20
NiII	$1.62 \pm 0.32 \times 10^{14}$	-0.31 ± 0.20	0.05 ± 0.20
Q 1037−270	$z_{\rm abs} = 2.139$		
FeII	$4.98 \pm 0.14 \times 10^{14}$	-0.32 ± 0.04	0.00 ± 0.00
SII	$6.05 \pm 0.15 \times 10^{14}$	0.00 ± 0.00	0.32 ± 0.04
SiII	$1.89 \pm 0.15 \times 10^{15}$	0.21 ± 0.08	0.53 ± 0.09
CrII	$1.02 \pm 0.58 \times 10^{13}$	-0.18 ± 0.57	0.14 ± 0.57
NiII	$6.43 \pm 1.04 \times 10^{13}$	0.05 ± 0.16	0.36 ± 0.16
MnII	$2.22 \pm 0.08 \times 10^{12}$	-0.70 ± 0.04	-0.37 ± 0.05
Q 1157+014	$z_{\rm abs} = 1.944$	[X/Zn]	
FeII	$2.95 \pm 0.08 \times 10^{15}$	-0.43 ± 0.04	0.00 ± 0.00
SiII	$1.00 \pm 0.01 \times 10^{16}$	0.06 ± 0.02	0.50 ± 0.03
ZnII	$1.09 \pm 0.02 \times 10^{13}$	0.00 ± 0.00	0.43 ± 0.04
CrII	$6.07 \pm 0.19 \times 10^{13}$	-0.29 ± 0.04	0.14 ± 0.04
NiII	$1.62 \pm 0.05 \times 10^{14}$	-0.43 ± 0.04	0.00 ± 0.04

Table 3. Total column densities and integrated abundance ratios relative to solar in the six DLAs of our sample.